Volume 12, Issue 3, Page 15-23, 2023 https://doi.org/10.46810/tdfd.1306573 Research Article

BİNGÖL ÜNİVERSİTESİ

Türk Doğa ve Fen Dergisi
Turkish Journal of Nature and Science

www.dergipark.gov.tr/tdfd

Effect of Longer Waiting Time During OCP and Pre-Applied Cleaning Potential In Corrosion Analysis of Zinc Metal

Salih CİHANGİR*

[1] Munzur University, Rare Earth Elements Application and Research Centre, Tunceli, Türkiye
[2] Munzur University, Department of Chemistry and Chemical Processes, Tunceli Vocational School, Tunceli, Türkiye
Salih CİHANGİR ORCID No: 0000-0001-5989-5230

**Corresponding author: salihcihangir@munzur.edu.tr*

(Received: 29.05.2023, Accepted: 12.07.2023, Online Publication: 27.09.2023)

Keywords
Zinc metal, SEM-EDS and XRD characterization, Tafel corrosion analysis, In-situ macro surface analysis,

Abstract: Tafel analysis is a widely accepted electrochemical technique for corrosion studies. A general literature search for one of the electronegative metals, zinc, revealed serious deviations in corrosion results. In order to understand the reasons behind these deviations, zinc metal was investigated at macro and micro levels during and after the Tafel corrosion analysis. In-situ macro surface investigation during the open circuit potential period and Tafel analysis were performed, and it was found that the zinc surface undergoes proceeding corrosion attack following the immersion in 3.5 wt.% NaCl solution. In-situ macro surface analysis exhibited that the pre-oxidation of the surface proceeds as nonuniform at local regions. SEM-EDS and XRD analysis proved that the particular crystal planes of the zinc form ZnO with increasing immersion time. A linear sweep voltammetry (LSV) technique was applied to detect the oxygen removal and starting hydrogen evolution potentials. Three identical Tafel experiments were performed on samples without any treatment, and another three consecutive Tafel experiments were performed on the samples which applied pre-reduction potential. Obtained results revealed that in-situ pre-applied reduction potential just before the Tafel analysis cleaned the surface and allowed uniform oxide formation, resulting in the lowest standard deviation of the calculated Tafel elements.

Çinko Metalinin Korozyon Analizinde OCP Sırasında Uzun Bekleme Süresinin ve Önceden Uygulanan Temizleme Potansiyelinin Etkisi

Anahtar Kelimeler
Çinko metal, SEM-EDS ve XRD karakterizasyonu, Tafel korozyon analizi, Yerinde makro yüzey analizi

Öz: Tafel analizi korozyon çalışmaları için yaygın olarak kabul edilen bir elektrokimyasal tekniktir. Elektronegatif metallerden biri olan çinko için genel bir literatür araştırması sonucu korozyon parametrelerinde ciddi sapmalar olduğu gözlemlenmiştir. Bu sapmaların arkasındaki nedenleri anlamak için Tafel korozyon analizi sırasında ve sonrasında çinko metali makro ve mikro seviyelerde incelenmiştir. Açık devre potansiyel süresi boyunca yerinde makro yüzey araştırması ve Tafel analizi yapılmış ve çinko yüzeyinin ağırlıkça %3.5 NaCl çözeltisine daldırıldıktan sonra devam eden korozyon ataklarına uğradığı tespit edilmiştir. Yerinde makro yüzey analizi, yüzeyin ön oksidasyonunun yerel bölgelerde tekdüze olmayan bir şekilde ilerlediğini göstermiştir. SEM-EDS ve XRD analizi, çinkonun belirli kristal düzlemlerinin artan daldırma süresi ile ZnO oluşturduğunu göstermiştir. Oksijen giderimi ve hidrojen oluşum potansiyellerini tespit etmek için lineer tarama voltametresi (LSV) tekniği uygulanmıştır. Herhangi bir işlem uygulanmadan numuneler üzerinde üç özdeş Tafel deneyi yapılmış ve ön indirgeme potansiyeli uygulan numuneler üzerinde ardışık üç Tafel deneyi daha yapıldı. Elde edilen sonuçlar Tafel analizinin yüzeyi temizlemesinden hemen önce yerinde önceden uygulanan numunelerde indirgeme potansiyeli ile homojen oksit oluşumuna sağlanmış ve hesaplanan Tafel elementlerinin oldukça düşük standart sapma ile tekrar edilebilir olduğu bulunmuştur.

1. INTRODUCTION

Zinc (Zn) is one of the most attractive materials in the literature. Zn alone was mentioned in the titles of approximately 4500 papers in 2022 and over 1300 papers in just the first quarter of 2023. While Zn is used in medical research for its effect on organisms [1], energy research for long-life metal batteries [2], and solar perovskite cells [3], micro-electronics research for semiconductors [4], Zn is also commonly used for anticorrosive surface preparation as standalone or in alloy structures [5-8]. Regardless of the main research focus of Zn-related studies, potentiodynamic corrosion investigations are widely employed. In the performed literature search, it was found a serious fluctuation of obtained corrosion parameters for especially zinc metal. For example, corrosion current densities in various Tafel studies (one of the most critical parameters in corrosion analysis) are reported as low as a few milliamperes per square to a few thousand milliamperes per centimeter square in various studies for Zn surfaces tested in 3.5 wt.% NaCl solution at 25°C is presented in Table 1.

Table 1. Obtained corrosion current densities of Zn metal in various studies.

The Method of Obtaining Zinc Metal Used for Corrosion Analysis	J_{corr}/ **µA cm^{-2}**
Electrodeposition [9]	10.60
Electrodeposition [10]	89.98
Pure Zn Sheet [11]	266.5
Pure Zn Sheet [12]	115
Electrodeposition [13]	11.23
Electrodeposition [14]	54.4
Electrodeposition [15]	28
Pure Zn Sheet [16]	~ 60
Pure Zn Sheet [17]	8442
Electrodeposition [18]	42
Electrodeposition [19]	8.91
Electrodeposition [20]	270
Electrodeposition (three different potentials) [21]	181.85 - 401.89
Electrodeposition (three different temperatures) [22]	8.94 - 182

It is a rather interesting outcome for a standardized corrosion measurement technique with quite fluctuated results. In fact, in corrosion measurements, the type of the surface phase also plays a critical role during the passivation in the anodic scan. However, there is an obvious pinpoint to explore for a better understanding and correct application of corrosion measurement. The reason behind this claim is the applied cleaning procedures of the surfaces before performing the corrosion experiment. In the literature, before corrosion, samples are polished with sandpapers by starting from 400 grids up to 3000- 5000 grids to get a finer polished surface. While it is practically impossible to reach two-dimensional (2D) flatness at the close or sub-micron level, the main purpose here is to assume the existence of a surface as possible as 2D because mathematical models developed for electrochemical processes are based on 2D space. In one aspect, if the surface energetics and the roughness of the metal count into account, it may likely be possible that corrosion attack only interacts outer layer (not with the sub or close micron holes) of the rough surfaces. While no direct study is encountered to support this claim, it is declared that there are two states called Cassie-Baxter and Wenzel for the surfaces subject to liquid contact [23]. The Cassie-Baxter state for rough surfaces is observed for most high-surface tension liquids, such as salty water (73 mN m^{-1} [24]). The Cassie-Baxter state supports that dry spaces are air-filled on rough surfaces in relatively higher surface tension liquids [25]. However, the dry locations in holes of rough surfaces do not tend to form when using low surface tension liquids, such as hexane (0.013 mN m^{-1} [26]). Therefore, it is undoubtedly expected to get more reliable results from well-polished surfaces. As discussed in the zinc case, reliable results are not always the case for even the corrosion tests of the same sample. In potentiodynamic scan (Tafel) analysis, the 15% deviation is declared as good reliability of the setup by leading potentiostat manufacturers because the contamination of the surface and the air-formed oxide, or even dissolved oxygen in the solution are expected to deviate the outcome. Moreover, the possibility of three-dimensional (3D) interaction of the corrosive solution with the surface is always in question, especially in insufficient polishing cases. In order to eliminate as possible as inflictive parameters on Tafel results, researchers mentioned applying pre-cleaning potential vs. reference or open circuit potential of the sample prior to the Tafel scan [27, 28]. Although sample preparation and cleaning processes were discussed, another important; unfortunately not as much considered parameter, the scan rate, is rather critical in corrosion experiments. While the most applied scan rate in the literature for Tafel corrosion experiments is between 0.1 mV s^{-1} and 1 mV s^{-1}, ASTM G5 (Standard Reference Test Method for Making Potentiodynamic Anodic Polarization Measurements) strongly recommends using 0.1667 mV s^{-1} as it allows sufficient time to protect the stable-state of the ongoing reactions still minimizing the capacitive current contribution [29]. Faster scan rate may be useful in particular cases, such as rather thin samples (less than a few microns), rapid dissolution and accumulation of the corroded species on the surface, or fast dealloying of the investigated alloy in question, to prevent the rapid degradation. In fact, the Tafel technique is based on the potential scan as applied in cyclic voltammetry (CV) and linear sweep voltammetry techniques (LSV), and it is known that higher scan rates always tend to decrease diffusion layer size and reveal higher current outputs [30, 31].

This study aims to investigate the effect of a long waiting time to reach the steady state condition (OCP) condition and applied pre-oxidation potential on corrosion parameters of Zn metal. In this approach, it will be observable if there are possible deviations in the Tafel parameters. Additionally, surfaces will also be examined at various stages for further understanding. Consequently, the study will be useful to the researchers for their Tafel corrosion experiments.

2. MATERIAL AND METHOD

All the chemicals were used as received. 3.5% wt. NaCl solution was prepared by a simple mixture of double-distilled water and NaCl salt (MERC). Employed potentiodynamic and potentiostatic experiments were carried out at room temperature with a three-electrode electrochemical workstation (Biologic, SP240) potentiostat. A pure zinc sheet (%99.9 pure, Alfa Aesar) was a working electrode. Standard Ag/AgCl (3.5M KCl, Gamry) glass frit-tip electrode was a reference electrode. The counter electrode was Ruthenium/Iridium coated Ti (40 cm^2 mesh electrode). A 3D-printed jacketed corrosion cell was used to standardize the Tafel experiments. Figure 1. Shows the photograph of the employed cell system in corrosion experiments. Before the corrosion experiment, samples were cleaned with 3000-4000 and 5000 grids polishing pads, washed with alcohol, and cleaned in ultrasound cleaner at 40 Hz for 2 minutes. The morphology and chemical composition of the deposited films were analyzed by scanning electron microscope (HITACHI SU3500, SEM) equipped with electron dispersive spectroscopy (EDS, Oxford Aztech) for elemental analysis. Energy dispersive X-ray (EDX, Oxford Inca) was used to analyze the crystal planes. XRD analysis was carried out using RIGAKU Miniflex 600 equipped with Cu Kα (λ = 1.788965 Å) radiation operated at 40 kV and 30 mA in 0,02° step size at 10-90°. In corrosion experiments, the Zn sheet served as a working electrode; Ag/AgCl (3.5 M KCl) electrode was used as the reference electrode; 25 cm^2 Ruthenium/Iridium coated Ti was used as a counter electrode. Stable open circuit potential (OCP) was observed before starting the Tafel analysis. For Tafel corrosion tests, a potentiodynamic voltammetric scan from -0.25 V_{OCP} to 0.25 V_{OCP} was performed at 0.166 mV s^{-1} scan rate.

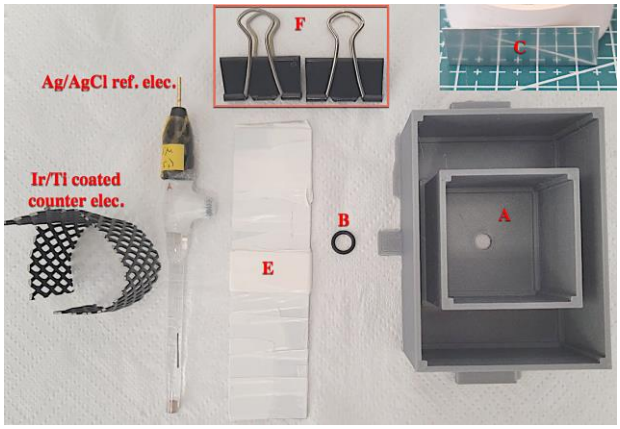

Figure 1. A (3D printed cell, PETG) is the topmost part, B (O-ring) is placed under the hole of A, and C (polished Zn substrate) is placed under B. Then, 1.5 mm thick, white electric tape-insulated SS-316 support (labeled as E) is placed under C. Binder clips (labeled as F) apply adequate pressure to support (E) and two side paddles of cell A. This way, the O-ring (B) and the main cell (A) are ready for a watertight operation. Reference and counter electrodes are placed inside the square corrosion chamber (A).

During corrosion experiments, a computer-controlled USB microscope was used for in situ observation of surface change to distinguish the macro surface changes depending on the applied potential. The images of the surfaces before the applied potential states and after the applied potential states were taken with a high-resolution material microscope equipped with a SONY-IMX485 camera and Mitutoyo optic lenses.

3. RESULTS AND DISCUSSION

If Tafel calculation is examined from obtained logarithmic current vs. potential graph, slopes for cathodic and anodic regions start from close points of the E_{corr}, as shown in Figure 2. As it is known, the sample does not corrode at the cathodic region in which hydrogen evolution reaction (HER) at the very negative potentials of starting cathodic slope takes place, but also Zn surface may reduce the oxygen by $O_2 + H_2O + 2e^- \rightarrow HO_2^- + OH^-$ in saline media [32]. At close points of the E_{corr} sample may initiate a weak nano/micro passivation region (usually rapidly breaks down) just before the anodic scan.

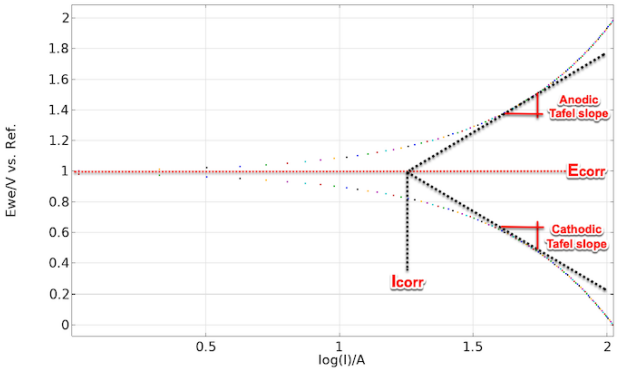

Figure 2. Anodic and cathodic lines are shown in a standard Tafel graph.

As mentioned, the mathematical models produced for initially heterogeneous electrochemical-based reactions (homogenous chemical redox transformation reactions may also occur) are usually based on 2D space. In order to properly fit the 2D mathematical approximation, it is important to evaluate the data that the surface does not significantly deviate from its initial geometrical state (tens of microns deep and wide cracking/pitting does not yet occur). Therefore, Tafel analysis generally uses the anodic and cathodic slopes of the region close to the E_{corr} value because the samples may undergo severe corrosion attack at far potential values of E_{corr}, especially in the anodic region. At more positive values from the E_{corr} at the anodic region, micro-cracks and holes are expected to occur for most surfaces. In this case, the surface moves away from its two-dimensional form, to which the mathematical model can be applied.

3.1 Investigation of Repetitive Open Circuit Potential Scan

OCP determination is applied for both Tafel and EIS corrosion studies, and various approaches are employed in different studies for stable OCP determination. In some studies, less than 20 mV deviation in 30 minutes is accepted as a sign of equilibrium before starting the corrosion analysis [33], and in a typical application, 30 minutes waiting time is declared as stable OCP deviation, usually without quantitative support of OCP deviation as a function of time [34-36]. Some groups also follow an

hour waiting time rule [37-39] because ASTM (American Society for Testing and Materials) states that an hour immersion time is required to reach the equilibrium state with an expected 10 mV h^{-1} or lower deviation [40]. In the former approach, the 20 mV s^{-1} deviation is a slightly higher value to accept as an equilibrium point or stable OCP because it corresponds to 40 mV h^{-1}. Still, the latter approach may also be detrimental to thin, less corrosion-resistant materials because chloride will continuously attack the surface once the sample is immersed in a corrosion solution. Then, the surface phase is eventually changed and prevents proper Tafel analysis. It is known that the reactions on the electrode surface take forever to reach a perfect equilibrium of infinite steady condition, but the point that these ongoing reactions proceed quite slowly and in near balance is accepted as equilibrium potential.

In order to overcome these issues, new-generation potentiostat devices provide an option for time-dependent potential change. In this option, even determined time is 2h for OCP, a limit function of time-dependent potential change (mV s^{-1}) is applied. If a limit function, for example, <0.1mV s^{-1}, the deviation is fulfilled before the 2h time condition, the Tafel scan starts. This way, good equilibrium (<10 mV h^{-1}) can be obtained, with unnecessary waiting time, and possible or further surface damage is prevented. In this study, three identical well-polished surfaces were prepared for OCP determination. The reference surface image of the prepared samples is shown in Figure 3. Then, samples were placed in the corrosion cell at room temperature for over 25 minutes until the observation of negligible deviation at OCP. This experiment was performed with two different approaches. The first approach was time-dependent, as mostly applied in the literature in which the sample was kept for a prolonged time (generally over 1000 s) to get stable OCP. The second approach was kinetic-based, as suggested by leading potentiostat manufacturers and in some literature studies. In the kinetic dependence, having <10 mV s^{-1} in the OCP measurement is strongly suggested.

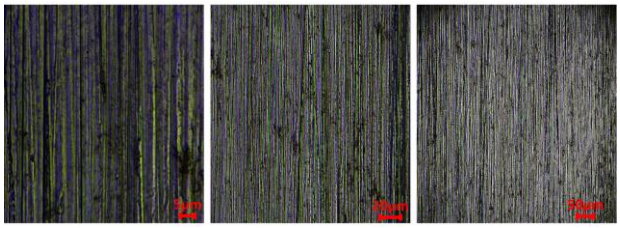

Figure 3. Before corrosion tests, the optical images of polished samples (presented in Figure 1. C) were taken. Scratches are expected to occur after polishing and were detected under a micron size.

In the first experiment, samples were observed for about 1800 s to reach a stable OCP value. Obtained OCP graphics are presented in Figure 4. In each performed OCP experiment, especially the last 300 s were more focused, and the deviation in the last 300 s was specifically sought for 10 mV h^{-1} or less.

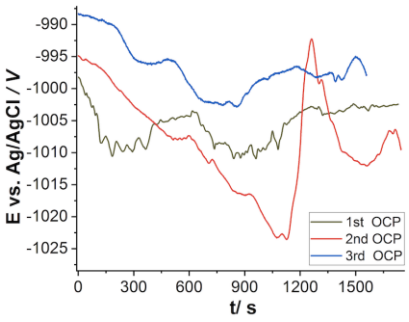

Figure 4. Three identical well-polished surfaces are placed in the corrosion cell and left for over 25 minutes until the observation of stable OCP behavior.

In the 1st OCP experiment, OCP was detected as -1002 $mV_{Ag/AgCl}$, and the deviation in the last 300 s was calculated as 6 mV h^{-1}. In the 2nd OCP experiment, OCP was detected as -1009 $mV_{Ag/AgCl}$, and the deviation in the last 300 s was calculated as 11 mV h^{-1}. In the 3rd OCP experiment, OCP was detected as -998$mV_{Ag/AgCl}$, and the deviation in the last 300 s was calculated as 1.2 mV h^{-1}. During the OCP experiments, a USB microscope camera system was set to observe macro surface changes, such as color alterations, bubble formations, etc. It was found interesting that the surface is expected to form ZnO with increasing immersion time during open circuit potential, as shown in Figure 5. because it is already reported in a comprehensive study that Zn initially tends to form ZnO at the early time of immersion along with the expected formation of $Zn(OH)_2$ for a prolonged time (over >10 hours) [32]. When obtained images at minutes 6 and 12 are compared, a clear color change is seen, and this color difference becomes more apparent at longer times, with a predominance at the edges. Initial surface corrosion products are formed following the immersion without any applied potential. In fact, formed oxide and hydroxide corrosion products creates a surface film resistant to further zinc corrosion, and thus, it is a protective result of the metal in corrosion media [32]. SEM-EDS and XRD carried out morphological and crystal plane investigations for the initial state and after the OCP state of the surfaces.

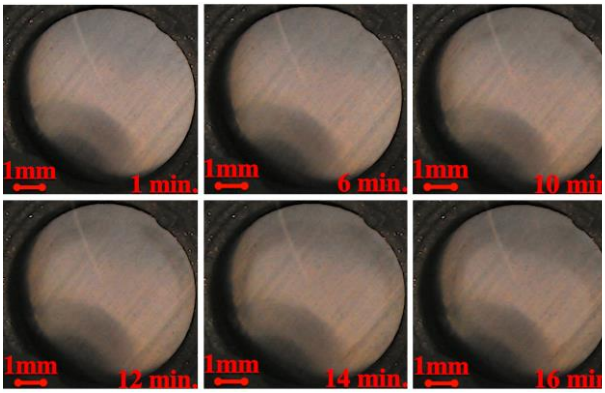

Figure 5. Macro surface images taken at various stages of the OCP period (as exhibited in Figure 4.) are presented.

In the SEM-EDS analysis, clean samples were first investigated. Then the sample employed OCP determination experiments for 1500 s and then examined with the SEM-EDS technique, as shown in Figure 6. When the pure Zn surface was investigated, it can be seen that the air-formed oxygen was equally distributed. EDS

analysis revealed 2.2% oxygen content. However, in the case of OCP-employed Zn surface, local blemishes were observed, oxygens were accumulated locally on the surface, and EDS analysis revealed a three-fold increase in oxygen content. An increase in oxygen content is expected due to the formation of ZnO and $Zn(OH)_2$. In the EDS analysis of OCP employed Zn, the right part of the sample, which, out of local blemished spot, more oxygen was detected.

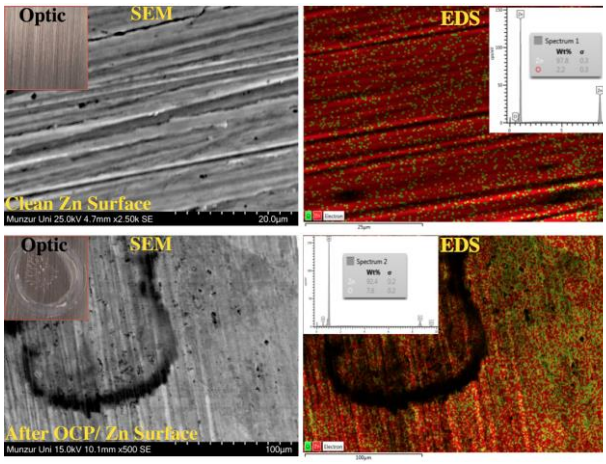

Figure 6. The electrochemically non-treated clean polished surface and the surface after the 1500 s OCP stage are investigated with SEM-EDS analysis.

In order to collect more data for the phenomenon of the initial formation of ZnO, XRD analysis was performed, as presented in Figure 7. The XRD data for pure ZnO powder was also presented in the XRD data graph. It is found that while all the peak intensities of the Zn (COD ID:9008522) decreased after the OCP stage, abrupt decreases in the intensity of (002) and (004) crystal planes were observed. Indeed, crystal planes analyzed after the OCP state became similar to that of (101) and (202) ZnO crystal planes (COD ID:2300112). In other words, the behavior at around 36° and 77° for OCP employed Zn started to resemble the (101) and (202) crystal planes of ZnO.

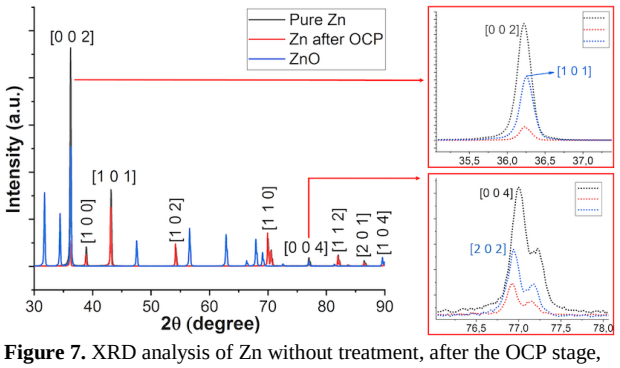

Figure 7. XRD analysis of Zn without treatment, after the OCP stage, and ZnO powder are presented.

When collected data in the optic microscope, SEM, EDS-mapping, and XRD are evaluated, it can be seen that the surface of the Zn starts to oxidize following the immersion and increases with immersion time. It was observed that the oxidation of the employed sample specifically preferred to occur in (004) and (101) crystal planes which are the most depressed crystal planes after OCP.

Following the OCP investigation, three identical Tafel experiments were performed on identical Zn surfaces. The Tafel polarization data with OCP graphs are presented in Figure 8. In the OCP analysis part, the potentiostat was adjusted to seek <10 mV h^{-1}.

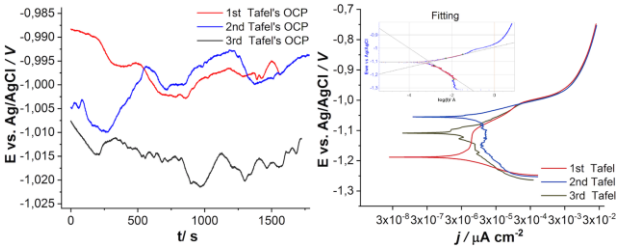

Figure 8. Three identical cleaned polished Zn sheets were observed for 1500 s in the OCP stage, and then the Tafel measurements were performed.

Biologic's advanced Tafel corrosion fit analysis program was used to obtain fitting parameters. Table 2 shows the obtained fitting parameters with mean and standard deviation values. Obtained E_{corr} and I_{corr} values match literature but deviate from each other. Normally, OCP and E_{corr} values are expected to be as possible as a match, but the 10% difference is still within the acceptable limit. The reason for the 10% deviation in E_{corr} values is explained in the OCP macro surface investigation section, given in Figure 5, in which the 3.5 wt.% NaCl medium caused changes on the surface with increasing immersion time before the actual Tafel scan took place.

Table 2. Tafel elements and the OCP data for performed experiments in Figure 8 are presented with mean and standard deviation values.

Samples	OCP/ mV	E_{corr}/ mV	J_{corr}/ µA cm^{-2}	βa/ mV	βc/ mV
1st sample	-998	-1189	2.667	164.7	345
2nd sample	-994	-1051	5.509	28.9	111
3rd sample	-1011	-1101	2.979	49	162
Mean	-1001	-1114	3.72	81	206
Standard Dev.	8.89	68.87	1.56	73.43	123.05

When Tafel polarization curves are examined, it can be seen that the cathodic curves deviate more than the anodic curves. Following the immersion and at the end of the cathodic part (close points to starting anodic region), the reaction (1) take place, as observed in the OCP stages and examined in XRD analysis. In other words, Zn already starts to oxidize with increasing immersion time.

$$Zn \rightarrow Zn^{2+} + 2e^{-} \quad (1)$$

In the Tafel analysis of the samples, before -1.2 V_{AgCl}, -1.05 V_{AgCl}, and -1.15 V_{AgCl} for the 1st, 2nd and, 3rd Tafel samples, respectively, hydrogen evolution given in reaction (2) takes place.

$$2H_2O + 2e^{-} \rightarrow 2OH^{-} + H_2 \quad (2)$$

While potential is scanning to more positive values in the cathodic region, oxygen consumption reactions (3) and (4) occur.

$$O_2 + H_2O + 2e^- \rightarrow HO_2^- + OH^- \quad (3)$$

$$HO_2^- + H_2O + 2e^- \rightarrow 3OH^- \quad (4)$$

If the surface is already oxidized, as observed in OCP experiments, and thus, the deviation at the cathodic region is expected to occur. In the final experiment, the surface of each sample is planned to be applied to a pre-potential for in-situ cleaning, and the OCP waiting times are kept under 600 s. In macro surface recorded OCP experiments, as discussed in Figure 5 and Figure 6 sections, the Zn surfaces were found to change at around 500 s. Moreover, in the OCP stage, the potentials at 500 s and 1500 s, given in Figure 8, were analyzed, and 1 mV difference for 1st Tafel sample (500 s: -997 mV and 1500 s: 997 mV), 3 mV difference for 2nd Tafel sample (500 s: -997 mV and 1500 s: 994 mV), and 2 mV difference for the 3rd Tafel sample (500 s: -1013 mV and 1500 s: 1011 mV) were detected. In other words, the potential values at 500 s, in which macro surface change does not evolve, were very close to the final OCP values at 1500 s. If the big picture is this, applied pre-potential along with shorter waiting time at the OCP stage may bring much more reliable results in Tafel corrosion tests.

In order to determine the correct potential which does not vigorously decompose the H_2O and damage the solution dynamics, a linear sweep voltammetry (LSV) experiment was performed at 0.2 mV s^{-1} scan rate after the OCP stage, as shown in Figure 9. Scan rate chosen as close as Tafel scan rate of 0.166 mV s^{-1}. Before the LSV scan, the OCP of the sample was determined, and then the linear voltammetry scan was started from 0 V_{OCP} to -500 mV_{OCP}. OCP of the samples was determined as -1034 mV, similar to those found in the Tafel experiments. The conspicuous thing is that the OCP value at 500 s was -1024 mV, which was acceptable to start the Tafel scan rather than waiting for an extra 1000 s to get -1034 mV. OCP and LSV curves of the Zn metal, along with macro surface images, are presented in Figure 9. The emerged peak at -300 mV_{OCP} (at -1.33 V) in LSV occurs mostly in reactions (3) and (4). However, the observed torsion after -1.4 V_{OCP} (more negative potentials) shows the starting of hydrogen evolution given in reaction (2).

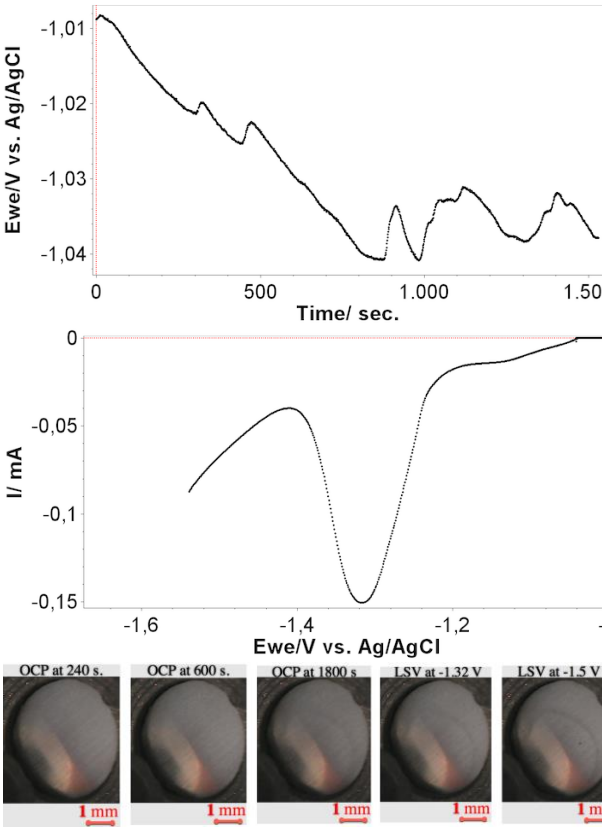

Figure 9. OCP and LSV graphs for the Zn working electrode are presented. The red line represents the zero-time baseline for OCP and the zero potential baselines for LSV.

If the macro surface images are investigated, it can be seen that the OCP image gets much darker through the end of the OCP (at 1800 seconds), forming shades on the surface. The observed darkness of the surface at the end of OCP started to disappear and became indistinct at -1.32 V of LSV, from which the peak emerged. Then, small hydrogen gas bubbles occurred at -1.5 V of the LSV scan.

In the next experiment, the sample was decided to be kept at OCP for 500 s because both performed experiments given Figure 5 and Figure 9 showed that longer waiting time causes oxide products that are not easy to dissolve. Moreover, 500 s and 1800 s of OCP have only a 1% difference. Following the OCP stage, samples are aimed to be applied a -600 mV potential difference (vs. V_{OCP}) to remove any air-formed oxide or reducible impurities. Then, after another 500 s OCP stage, the Tafel test was employed. In this way, it is aimed to obtain a more reliable and repeatable corrosion testing procedure. Pre-applied potential-based Tafel analysis is presented in Figure 10 with relevant macro surface images at the end of each stage.

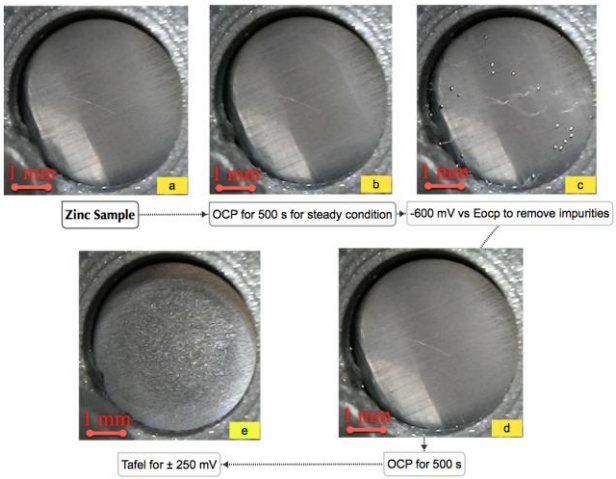

Figure 10. a represents the polished zinc surface in the corrosion solution, b represents the 500 s OCP stage, c represents the -600 mV vs. EOCP potential, d represents the OCP stage before Tafel, and e represents the surface in the corrosion solution following the Tafel.

One of the interesting findings in pre-applied potential-based Tafel analysis was observed in the OCP stage shown in Figure 10d. There was no locally formed blemished area with 500 s OCP stage, as it was observed in the OCP stage for 1800 s in Figure 9. The surface was quite uniform, and any possible impurities were removed during the applied -600 mV potential, given in Figure 10c. A clear white blemishing shade, normally, appeared in Figure 10b., was disappeared in Figure 10c. It was, in fact, an expected result because applied reduction potential removed the formed oxide layer along with any other impurities during hydrogen evolution. Moreover, nearly a perfectly uniform surface behavior at OCP before Tafel in Figure 10d emerged as a great improvement. If pre-applied potential-based Tafel analysis and Tafel analysis without pre-applied reduction potential are compared, it can be said that no other surface cleaning procedure, such as polishing, ultrasound cleaning, or alcohol cleaning, is effective as the in-situ surface cleaning procedure. In order to understand the effect of in-situ surface cleaning on the Tafel analysis, three repetitive experiments were performed in the given order in Figure 10, and it is presented in Figure 11.

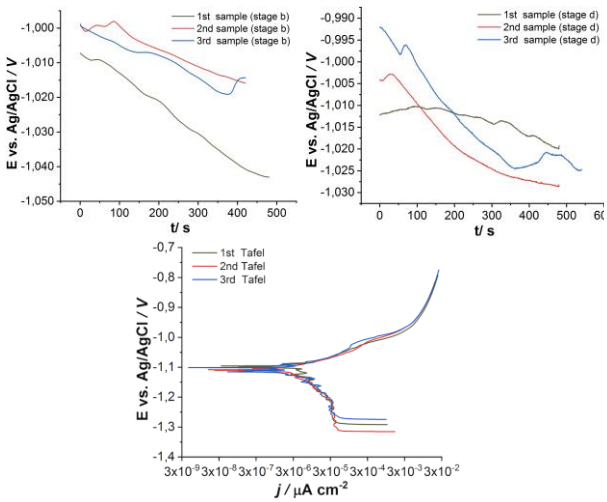

Figure 11. Three repetitive experiments at stage b and stage d for OCP, given in Figure 10, are presented with repetitive Tafel polarization curves.

Obtained curves are rather consistent when compared with the direct Tafel analysis in Figure 8. The calculated mean and standard deviation analysis in Table 2 shows a significant match between repetitive experiments.

Table 3. Tafel fitting elements for each sample are presented for performed repetitive experiments given in Figure 11.

Samples	OCP/ mV	E_{corr}/ mV	J_{corr}/ µA cm^{-2}	βa/ mV	βc/ mV
1 st Tafel	-1027	-1106	1.94	37.2	84
2 nd Tafel	-1025	-1105	2.32	35.6	99
3 rd Tafel	-1020	-1107	2.77	47	103
Mean	-1024	-1106	2.34	39.93	95.33
Standard Dev.	3.60	1	0.41	6.17	10.01

If each component of the pre-applied potential-based Tafel analysis given in Table 2 and the direct Tafel analysis given in Table 1 are compared, a slight deviation in each parameter is seen as contrary to Table 1. However, two of the most important kinetic parameters, βa, and βc, are consistent because providing similar results in βa and βc is normally difficult compared to the Ecorr and Jcorr values. Almost every experiment revealed identical results. As mentioned, the obtained consistent results likely emerge from equalizing the starting conditions of each surface in in-situ via applied moderate reduction potential. This way, a uniform oxidation process at the relaxed OCP state while reaching the steady state condition and during the potentiodynamic scan is provided.

4. CONCLUSIONS

The study questioned the deviation for Tafel corrosion analysis results of Zinc metal in various reports. Also, rarely applied in-situ surface cleaning potential before Tafel analysis was investigated in detail. This study has shown that pre-applied surface cleaning reduction potential before Tafel can improve the consistency and repeatability of the experiments. Macro surface investigation and EDS/XRD analysis prove that surface oxidation is initiated upon immersion and increases in time, and the oxidation of the surface does not proceed at the same rate through the surface. This non-uniform behavior is likely the result of surface impurities, such as air oxidation of the surface and other pre-existed impurities. However, after determining the correct cleaning potential via LSV and applying the determined potential prior to Tafel to clean the surface revealed remarkable results in terms of repeatability and consistency of the Tafel parameters. A few general trends can be written if the performed study is translated to other metals investigated for Tafel analysis.

- As the corrosion medium starts to change the surface with increasing immersion time, the optimum OCP period can be decided after a few consecutive OCP experiments, and the optimum time can be chosen as the shortest time, which is the closest time to the long OCP analysis.

- Prior to Tafel analysis, LSV analysis following the OCP analysis can be performed to detect the oxide removal potential and starting potential for hydrogen evolution.

- The sample can be applied in-situ reduction potential to remove the oxide layer and other uncounted impurities to obtain a standardized surface before Tafel analysis.

Acknowledgement

I would like to thank The Scientific and Technological Research Council of Turkey (TUBITAK) (grant no. 120Z733) for their support in carrying out the study.

REFERENCES

[1] L.H. Jørgensen, M.D. Sørensen, M.M. Lauridsen, L. Rasmussen, R.M. Alfiler, V.N. Iversen, O.B. Schaffalitzky de Muckadell, Albumin-corrected Zn and available free Zn-binding capacity as indicators of Zn status–potential for clinical implementation, Scandinavian Journal of Clinical and Laboratory Investigation. 2022;82(4):261-266.

[2] Z. Huang, Z. Li, Y. Wang, J. Cong, X. Wu, X. Song, Y. Ma, H. Xiang, Y. Huang, Regulating Zn (002) Deposition toward Long Cycle Life for Zn Metal Batteries, ACS Energy Letters. 2022;8(1):372-380.

[3] M. Badrooj, F. Jamali-Sheini, N. Torabi, Zn-doped Pb/Sn hybrid perovskite solar cells: Towards high photovoltaic performance, Solar Energy. 2022;236:63-74.

[4] X. Xie, J. Zhao, O. Lin, Z. Yin, X. Li, Y. Zhang, A. Tang, Narrow-Bandwidth Blue-Emitting Ag–Ga–Zn–S Semiconductor Nanocrystals for Quantum-Dot Light-Emitting Diodes, The Journal of Physical Chemistry Letters. 2022;13:11857-11863.

[5] H. Jia, M. Wang, S. Luo, The corrosion behaviour of a novel Mg–Zn–Zr–Y–Cu alloy, Materials Science and Technology. 2023:1-8.

[6] W. Wu, G. Sun, Q. Wang, S. Lin, Preparation, Wear Resistance, and Corrosion Performance of Arc-Sprayed Zn, Al, and Zn-Al Coatings on Carbon Steel Substrates, Journal of Materials Engineering and Performance. 2023:1-14.

[7] S. Huang, W. Wu, G. Han, L. Wang, X. Mei, L. Qiao, Y. Yan, Revealing the corrosion product films of ion-implanted biodegradable Zn–Cu alloys, Corrosion Science. 2023;210:110814.

[8] R.E. Hammam, S.A. Abdel-Gawad, M.E. Moussa, M. Shoeib, S. El-Hadad, Study of Microstructure and Corrosion Behavior of Cast Zn–Al–Mg Alloys, International Journal of Metalcasting. 2023:1-14.

[9] K. Baldwin, C. Smith, Advances in replacements for cadmium plating in aerospace applications, Transactions of the IMF. 1996;74(6):202-209.

[10] A. El Fazazi, M. Ouakki, M. Cherkaoui, Electrochemical Deposition and Spectroscopy Investigation of Zn Coatings on Steel, Journal of Bio-and Tribo-Corrosion. 2021;7:1-22.

[11] L. Hao, G. Lv, Y. Zhou, K. Zhu, M. Dong, Y. Liu, D. Yu, High performance anti-corrosion coatings of poly (vinyl butyral) composites with poly n-(vinyl) pyrrole and carbon black nanoparticles, Materials. 2018;11(11):2307.

[12] H.M. Abd El-Lateef, E.-S. Abdel-Rahman, H.S. Mohran, Role of Ni content in improvement of corrosion resistance of Zn–Ni alloy in 3.5% NaCl solution. Part I: Polarization and impedance studies, Transactions of Nonferrous Metals Society of China. 2015;25(8):2807-2816.

[13] K. Vathsala, T.V. Venkatesha, Zn–ZrO2 nanocomposite coatings: elecrodeposition and evaluation of corrosion resistance, Applied Surface Science. 2011;257(21):8929-8936.

[14] M.M.K. Azar, H.S. Gugtapeh, M. Rezaei, Evaluation of corrosion protection performance of electroplated zinc and zinc-graphene oxide nanocomposite coatings in air saturated 3.5 wt.% NaCl solution, Colloids and Surfaces A: Physicochemical and Engineering Aspects. 2020;601:125051.

[15] S. Ganesan, G. Prabhu, B.N. Popov, Electrodeposition and characterization of Zn-Mn coatings for corrosion protection, Surface and Coatings Technology. 2014;238:143-151.

[16] J. Wang, Y. Qi, X. Zhao, Z. Zhang, Electrochemical investigation of corrosion behavior of epoxy modified silicate zinc-rich coatings in 3.5% NaCl solution, Coatings. 2020;10(5):444.

[17] M. Sudha, S. Surendhiran, V. Gowthambabu, A. Balamurugan, R. Anandarasu, Y.A. Syed Khadar, D. Vasudevan, Enhancement of Corrosive-Resistant Behavior of Zn and Mg Metal Plates Using Biosynthesized Nickel Oxide Nanoparticles, Journal of Bio- and Tribo-Corrosion. 2021;7(2):60.

[18] S. Ranganatha, T. Venkatesha, Fabrication and electrochemical characterization of Zn–halloysite nanotubes composite coatings, RSC Advances. 2014;4(59):31230-31238.

[19] A. Yavuz, P. Yilmaz Erdogan, H. Zengin, G. Zengin, Electrodeposition and Characterisation of Zn-Co Alloys from Ionic Liquids on Copper, Journal of Electronic Materials. 2022;51(9):5253-5261.

[20] F. Azizi, A. Kahoul, Electrodeposition and corrosion behaviour of Zn–Co coating produced from a sulphate bath, Transactions of the IMF. 2016;94(1):43-48.

[21] R. Kumar Swain, P. Upadhyay, A. Nag, A. Banerjee, A.N. Bhagat, A. Basu, A. Mallik, Electro-galvanization of zinc and zinc-nickel onto mild steel for improved corrosion resistance, Materials Today: Proceedings. 2022;62:6257-6264.

[22] K. Sai Jyotheender, M.K. Punith Kumar, C. Srivastava, Low temperature electrogalvanization: Texture and corrosion behavior, Applied Surface Science. 2021;559:149953.

[23] B.M.L. Koch, A. Amirfazli, J.A.W. Elliott, Wetting of Rough Surfaces by a Low Surface Tension Liquid, The Journal of Physical Chemistry C. 2014;118(41):23777-23782.

[24] V. Vinš, J. Hykl, J. Hrubý, Surface tension of seawater at low temperatures including supercooled region down to–25 C, Marine Chemistry. 2019;213:13-23.

[25] S.K. Behera, A. Kumar P, N. Dogra, M. Nosonovsky, P. Rohatgi, Effect of Microstructure on Contact Angle and Corrosion of Ductile Iron: Iron–Graphite Composite, Langmuir. 2019;35(49):16120-16129.
[26] B. Grigoryev, B. Nemzer, D. Kurumov, J. Sengers, Surface tension of normal pentane, hexane, heptane, and octane, International journal of thermophysics. 1992;13:453-464.
[27] H. Luo, H. Su, C. Dong, X. Li, Passivation and electrochemical behavior of 316L stainless steel in chlorinated simulated concrete pore solution, Applied Surface Science. 2017;400:38-48.
[28] Li, O.J. Swanson, G.S. Frankel, A.Y. Gerard, P. Lu, J.E. Saal, J.R. Scully, Localized corrosion behavior of a single-phase non-equimolar high entropy alloy, Electrochimica Acta. 2019;306:71-84.
[29] N. Elgrishi, K.J. Rountree, B.D. McCarthy, E.S. Rountree, T.T. Eisenhart, J.L. Dempsey, A Practical Beginner's Guide to Cyclic Voltammetry, Journal of Chemical Education. 2018;95(2):197-206.
[30] A.J. Bard, L.R. Faulkner, Fundamentals and applications, Electrochemical methods. 2001;2(482):580-632.
[31] J.-M. Savéant, Elements of molecular and biomolecular electrochemistry: an electrochemical approach to electron transfer chemistry, John Wiley & Sons2006.
[32] Y. Meng, L. Liu, D. Zhang, C. Dong, Y. Yan, A.A. Volinsky, L.-N. Wang, Initial formation of corrosion products on pure zinc in saline solution, Bioactive materials. 2019;4:87-96.
[33] Y.F. Cherneikina, Ruzil; Kulyasova, Olga; Mingo, Beatriz; Mukaeva, Veta; Parfenov, Evgeny; Yerokhin, Aleksey, Microstructure effects on corrosion behaviour of Mg-1Ca alloy in Ringer's solution, Mendeley_Data 2019;http://dx.doi.org/10.17632/ccrp8sc3sj.1
[34] J.D. Brassard, D.K. Sarkar, J. Perron, A. Audibert-Hayet, D. Melot, Nano-micro structured superhydrophobic zinc coating on steel for prevention of corrosion and ice adhesion, Journal of Colloid and Interface Science. 2014;447(1095-7103 (Electronic)):240-247.
[35] C. Xiang, Z.M. Zhang, H.M. Fu, E.H. Han, H.F. Zhang, J.Q. Wang, Microstructure and corrosion behavior of AlCoCrFeNiSi0.1 high-entropy alloy, Intermetallics. 2019;114:106599.
[36] H. Luo, Z. Li, A.M. Mingers, D. Raabe, Corrosion behavior of an equiatomic CoCrFeMnNi high-entropy alloy compared with 304 stainless steel in sulfuric acid solution, Corrosion Science. 2018;134:131-139.
[37] Z.B. Wang, H.X. Hu, Y.G. Zheng, Synergistic effects of fluoride and chloride on general corrosion behavior of AISI 316 stainless steel and pure titanium in H2SO4 solutions, Corrosion Science. 2018;130:203-217.
[38] Q. Ye, K. Feng, Z. Li, F. Lu, R. Li, J. Huang, Y. Wu, Microstructure and corrosion properties of CrMnFeCoNi high entropy alloy coating, Applied Surface Science. 2017;396:1420-1426.
[39] Z. Cui, L. Wang, H. Ni, W. Hao, C. Man, S. Chen, X. Wang, Z. Liu, X. Li, Influence of temperature on the electrochemical and passivation behavior of 2507 super duplex stainless steel in simulated desulfurized flue gas condensates, Corrosion Science. 2017;118:31-48.
[40] A. International, ASTM G59-97, Standard Test Method for Conducting Potentiodynamic Polarization Resistance Measurements, ASTM West Conshohocken, PA, 2014.